SOURCE
DATA

TRANSPARENT
PROCESS

YTHDF1-mediated translation amplifies Wnt-driven intestinal stemness

Bing Han[1,†], Sujun Yan[1,†], Saisai Wei[1,†], Jie Xiang[1], Kangli Liu[1], Zhanghui Chen[2], Rongpan Bai[3], Jinghao Sheng[3], Zhengping Xu[3] & Xiangwei Gao[1,3,*] iD

Abstract

N6-methyladenosine (m^{6}A) mRNA methylation has emerged as an important player in many biological processes by regulating gene expression. However, its roles in intestinal stem cell (ISC) homeostasis remain largely unknown. Here, we report that YTHDF1, an m^{6}A reader, is highly expressed in ISCs and its expression is upregulated by Wnt signaling at the translational level. Whereas YTHDF1 is dispensable for normal intestinal development in mice, genetic ablation of *Ythdf1* dramatically blocks Wnt-driven regeneration and tumorigenesis with reduced ISC stemness. Mechanistically, YTHDF1 facilitates the translation of Wnt signaling effectors including *TCF7L2/TCF4*, while this process is enhanced during Wnt activation to augment β-catenin activity. Targeting YTHDF1 in ISCs of established tumors leads to tumor shrinkage and prolonged survival. Collectively, our studies unveil YTHDF1 as an amplifier of Wnt/β-catenin signaling at the translational level, which is required for the maintenance of ISCs during regeneration and tumorigenesis.

Introduction

The intestinal epithelium harbors remarkable self-renewal capacity driven by the intestinal stem cells (ISCs) at the intestinal crypts [1]. The canonical Wnt/β-catenin (CTNNB1) signaling pathway is one of the key regulators of intestinal stemness, which is responsible for the control of intestinal homeostasis, regeneration, and tumorigenesis [2]. Under physiological condition, Wnt activity is tightly regulated to form a gradient in the intestinal crypt, which is essential for the undifferentiated state of ISCs and epithelium homeostasis [2]. In

response to intestine damage, this signaling is activated to drive tissue regeneration [3]. The aberrant activation of Wnt/β-catenin signaling, frequently observed in colorectal cancer (CRC) patient samples, leads to the development of CRC [4,5]. As the central signal transducer of Wnt pathway, β-catenin protein is tightly regulated. In the absence of a Wnt signal, the cytosolic levels of β-catenin are kept low by the destruction complex including axin, adenomatous polyposis coli (APC), and glycogen synthase kinase 3β (GSK3β). Wnt activation disrupts this complex, resulting in the translocation of β-catenin to the nucleus, where it associates with the T-cell factor/lymphoid enhancer factor (TCF/LEF) family of transcription factors to activate transcription of downstream target genes [2]. Although stabilization and localization of β-catenin contribute to its activation, other layers of Wnt/β-catenin signaling regulation remain to be characterized.

Recent studies point to a role of the mRNA methylation in the regulation of gene expression. In eukaryotic cells, one abundant and conserved mRNA modification is adenosine methylation at the nitrogen-6 position, N6-methyladenosine (m^{6}A). The biological effects of m^{6}A methylation are mediated by "writer", "eraser", and "reader" proteins. The RNA methyltransferase complex, mainly consisting of METTL3, METTL14, and WTAP, catalyzes the m^{6}A methylation of mRNA [6–8]. FTO and ALKBH5 have been identified to mediate the reversible removal of this methylation [9,10]. In addition, the YTH domain family proteins serve as the major m^{6}A-binding proteins to regulate RNA metabolism, including mRNA splicing, degradation, and translation [11–14]. Through regulating gene expression, m^{6}A methylation plays important roles in a diverse array of biological processes [15].

m^{6}A mRNA methylation is emerging as a crucial modulator in regulating the pluripotency of stem cells, while the overall impact of this modification in stem cell biology is complex. For instance, knockout of *Mettl3* impairs the differentiation of mouse embryonic stem cells (ESCs) as well as hematopoietic stem cells (HSCs), indicating that m^{6}A promotes stem cell differentiation [16–18]. However, m^{6}A modification was also reported to be required for the pluripotency maintenance of human ESCs and HSCs [19,20]. These inconsistent results could be attributed to the cell-type-specific expression of the "writers", "erasers", and "readers". Moreover, the

1 Institute of Environmental Medicine, Sir Run-Run Shaw Hospital, Zhejiang University School of Medicine, Hangzhou, China
2 Affiliated Hospital of Guangdong Medical University, Zhanjiang, China
3 Bioelectromagnetics Laboratory of Zhejiang Province, Zhejiang University School of Medicine, Hangzhou, China
*Corresponding author. Tel: +86 571 88208169; Fax: +86 571 88208169; E-mail: xiangweigao@zju.edu.cn
†These authors contributed equally to this work

effects of m[6]A reader proteins are pleiotropic as YTHDF1 promotes the translation whereas YTHDF2 facilitates the degradation of methylated mRNAs, making the outcome more complicated [11–14]. To date, the roles of various m[6]A reader proteins in the maintenance of stem cell features remain largely unexplored.

In this study, we systematically investigated the function of YTHDF1 in the gut. Our results indicated that YTHDF1 plays an indispensable role in the activation of β-catenin to sustain ISC characteristics during regeneration and tumorigenesis.

Results

Wnt signaling promotes YTHDF1 expression at the translational level

m[6]A-dependent gene expression regulation plays critical roles in a variety of biological processes [15]. To investigate the possible function of m[6]A modification in Wnt-regulated intestinal homeostasis, we activated Wnt signaling in mouse intestinal crypt and examined the expression of m[6]A machinery. Wnt3a treatment slightly increased METTL3 expression, implying the involvement of m[6]A in Wnt signaling. Focusing on m[6]A reader proteins, we found that YTHDF1 protein level was dramatically induced by Wnt3a (Fig 1A). *Ythdf1* mRNA level was not affected by Wnt3a stimulation (Fig EV1A). Polysome profiling revealed that *Ythdf1* mRNA distribution in polysome fractions dramatically increased after Wnt3a treatment (Fig 1B), indicating the activated translation. Inactivating mutations in *APC* causes constitutive activation of β-catenin. To examine the regulation of YTHDF1 expression by *APC* mutation, we re-introduced wild-type full-length APC using the lentivirus system in SW620 human CRC cells, which express a non-functional truncated APC protein [4]. Overexpression of APC caused a significant reduction in YTHDF1 protein without affecting its mRNA level (Figs 1C and EV1B). YTHDF1 protein was relatively stable even after 12 h of translation inhibition with cycloheximide (CHX), excluding the possibility of protein degradation (Fig EV1C). Polysome profiling confirmed that APC perturbation mainly affected *YTHDF1* mRNA translation (Fig 1D). The 5′ untranslated regions (5′UTRs) play essential roles in mRNA translation [21]. Luciferase assay demonstrated that APC expression in SW620 cells dramatically decreased the translation mediated by the 5′UTR of *YTHDF1* mRNA (Fig 1E). To test whether YTHDF1 was regulated by β-catenin, we silenced β-catenin expression in SW620 cells using siRNAs and detected no obvious change in YTHDF1 expression (Fig EV1D and E). Reciprocally, expression of a non-degradable β-catenin mutant (N90) into RKO cells, whose APC/β-catenin pathway is intact, did not affect YTHDF1 expression (Fig EV1F and G), indicating that YTHDF1 is not regulated by β-catenin. Collectively, our data demonstrated that Wnt ligand treatment or APC mutation but not β-catenin promotes YTHDF1 expression.

Since mutations in *APC* are frequently observed in CRC [5,22], we examined whether YTHDF1 expression was altered in mouse and human intestinal tumors. We found that YTHDF1 protein was weakly expressed in the mouse intestinal tissue while sharply upregulated following *Apc* mutation (*Apc^{min/+}*). High YTHDF1 expression was maintained in intestinal adenomas from the *Apc^{min/+}* mice but not in adjacent non-tumor tissue (Figs 1F and EV1H).

Immunohistochemical staining revealed that YTHDF1 protein level is ubiquitously higher in CRC tissues than that in adjacent non-tumor tissues (Figs 1G and EV1J and K). TCGA datasets revealed upregulation of YTHDF1 expression in CRC (Fig EV1L). These results suggested that an increase in YTHDF1 might play an oncogenic role in intestinal tumorigenesis.

YTHDF1 is required for intestinal epithelial regeneration

In order to assess the function of intestinal epithelial YTHDF1, we generated a *Ythdf1* conditional knockout mouse strain under the villin promoter (*Villin^{Cre/+}:Ythdf1^{fl/fl}*, termed as *Ythdf1^{cKO}*) by targeting exon 4 (Fig EV2A–C). To determine the *in vivo* implications of YTHDF1 in normal intestinal homeostasis, intestinal architecture and body weight were evaluated in wild-type (*Ythdf1^{CTL}*) and *Ythdf1^{cKO}* mice at 8 weeks of age. The ablation of *Ythdf1* in intestinal epithelium did not affect body mass (Fig EV2D), crypt–villus architecture, and epithelial cell proliferation (Figs 2A and EV2E–H). Alkaline phosphatase staining (enterocytes) and Alcian blue staining (goblet cells) did not show significant difference between *Ythdf1^{CTL}* and *Ythdf1^{cKO}* intestine (Fig EV2I). Thus, YTHDF1 is largely dispensable for intestinal homeostasis under physiological condition.

The ability of the intestinal epithelium to regenerate after challenge is a Wnt-driven process that mimics the proliferation observed after *Apc* deletion [22,23]. We, therefore, examined YTHDF1 expression in response to intestinal injury. Mice were exposed to 12 Gy whole-body γ-irradiation (IR), and then, YTHDF1 expression was examined at various time points during the recovery phase. YTHDF1 protein level was markedly upregulated 3 days post-IR during which regenerative proliferation from the radio-resistant ISCs initiated, and then returned to baseline levels within 1 week (Fig 2B). The expression pattern of YTHDF1 was much similar to c-Myc, a proliferation marker (Fig 2B). Immunohistochemistry revealed that YTHDF1-expressing cells were located in the regenerative foci known to exhibit high Ki67 expression (Fig 2C). Together, these data suggested the induction of YTHDF1 during regeneration.

Given the dynamic changes of YTHDF1 expression in response to irradiation, we considered that YTHDF1 may play a role during intestinal regeneration. In *Ythdf1^{CTL}* mice, small intestine regeneration was characterized by a rapid renewal of intestinal crypts, which could be seen 72 h following 12 Gy whole-body IR (Fig 2D). By comparison, *Ythdf1^{cKO}* mice showed a clear defect in recovery capability which was highlighted by a significant reduction in both the amount and size of regenerating crypts (Fig 2D). Moreover, a remarkably reduced amount of Ki67-positive cells was manifested within the *Ythdf1^{cKO}* intestinal crypts (Fig 2D). Knockout of *Ythdf1* significantly reduced the expression of Wnt target genes including *Lgr5*, *Fzd7*, and *Myc* (Fig 2E) [24,25]. Taken together, these data suggested that YTHDF1 within the intestinal epithelium is critical for Wnt-driven intestinal regeneration.

Ythdf1 deletion reduces Wnt-driven tumorigenesis *in vivo*

Given that YTHDF1 was upregulated in intestinal tumors, we examined the function of YTHDF1 in Wnt-driven tumorigenesis using the *Apc^{min/+}* mouse model. Deficiency of YTHDF1 dramatically reduced intestinal tumor formation (Fig 3A). Both tumor number and tumor load were significantly diminished in *Ythdf1*-deleted mice (Fig 3B
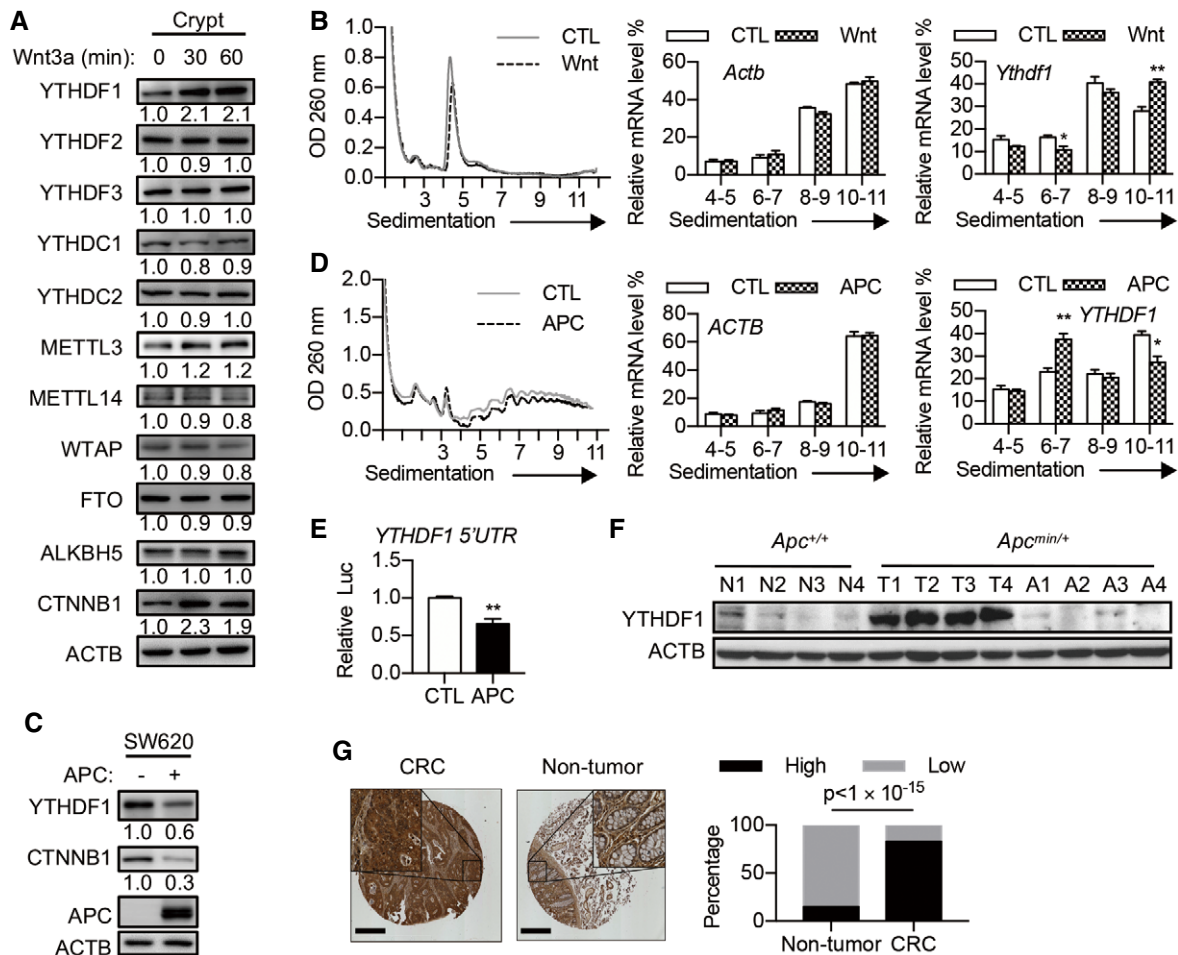
Figure 1. Wnt signaling promotes YTHDF1 expression at the translational level.

A Immunoblot analysis of mouse intestinal crypts treated with Wnt3a (60 ng/ml) for indicated time. The relative protein level was quantified and shown under each band.

B Polysome profiles of mouse intestinal crypt treated with or without Wnt3a for 30 min. The right panels show the distributions of *Ythdf1* and *Actb* in polysome fractions. Data are represented as mean ± SEM. *$P < 0.05$, **$P < 0.01$ (3 biological replicates, *t*-test).

C Immunoblot analysis of SW620 cells with or without APC overexpression. The relative protein level was quantified and shown under each band.

D Polysome profiles of SW620 cells with or without APC overexpression. The right panels show the distributions of *YTHDF1* and *ACTB* in polysome fractions. Data are represented as mean ± SEM. *$P < 0.05$, **$P < 0.01$ (3 biological replicates, *t*-test).

E Dual-Luciferase Assay with a construct bearing the 5′UTR of *YTHDF1* in SW620 cells with or without APC overexpression. Data are represented as mean ± SEM. *$P < 0.05$, **$P < 0.01$ (3 biological replicates, *t*-test).

F YTHDF1 protein expression in intestinal tissue from 4 pairs of $Apc^{+/+}$ and $Apc^{min/+}$ mice. N, normal tissue. T, tumor tissue. A, tumor-adjacent tissue.

G YTHDF1 staining in matched samples of human CRC tissue and adjacent non-tumor tissue. Scale bar, 450 μm. The right panel shows the statistics of IHC scores. Chi-square test; $n = 75$ for each group.

Source data are available online for this figure.

and C). Furthermore, analysis of tumor-size distribution showed that most of the tumors in *Ythdf1*-deleted mice were smaller in size (Fig 3D).

To further confirm the results in $Apc^{min/+}$ mouse model, we employed another CRC model induced by azoxymethane (AOM)/dextran sulfate sodium (DSS) (Fig 3E). In this model, mice develop CRC as the result of mutations in several genes including β-catenin pathways [26]. In AOM/DSS-induced tumor, YTHDF1 expression is upregulated (Fig EV1I). Similar to the $Apc^{min/+}$ model, decreased tumor number, tumor load, and size were observed in $Ythdf1^{cKO}$ mice compared to the wild-type group (Fig 3F–I). These data

highlighted the necessity of YTHDF1 in Wnt-driven intestinal tumor development.

YTHDF1 is required for maintenance of mouse intestinal stem cells

To start exploring the mechanism of YTHDF1-promoted intestinal tumorigenesis, we examined the YTHDF1 expression pattern in the intestine. *In situ* hybridization revealed that *Ythdf1* mRNA was predominantly localized in crypts, where the ISCs reside (Fig 4A). Consistently, fractionating primary intestinal tissue into
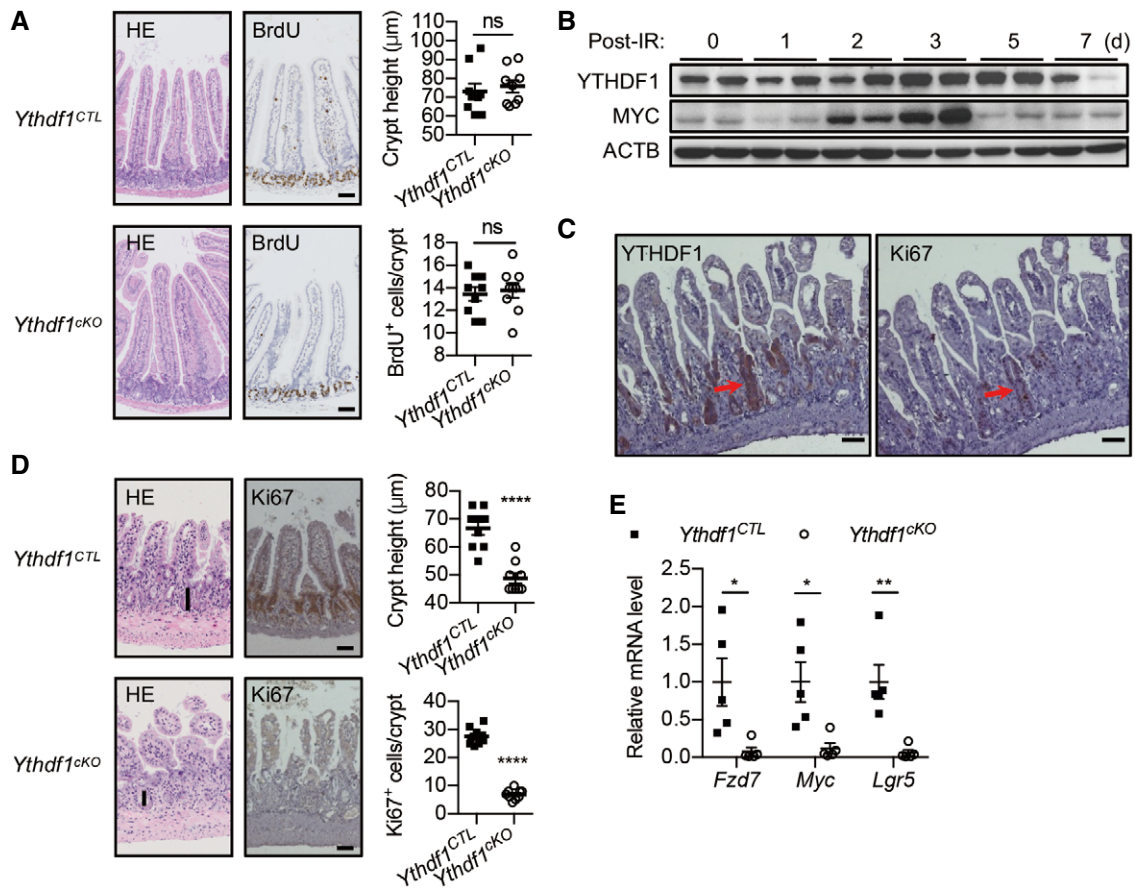
Figure 2. YTHDF1 is required for efficient intestinal regeneration.

A   The representative jejunum from wild-type (Ythdf1^CTL) and Ythdf1^cKO mice. Left: hematoxylin and eosin staining (H&E); middle: BrdU staining; right: quantification of crypt height and BrdU+ cells. Scale bar, 50 μm. Data are represented as mean ± SEM. (9 biological replicates, t-test).

B   Immunoblot analysis of small intestines from Ythdf1^CTL and Ythdf1^cKO mice after 12 Gy IR.

C   YTHDF1 (left) and Ki67 (right) staining of small intestine from wild-type mice 72 h after 12 Gy IR. Scale bar, 50 μm. Red arrows indicate the proliferating cells.

D   Small intestines from Ythdf1^CTL and Ythdf1^cKO mice 72 h after 12 Gy IR. Left: H&E staining; middle: Ki67 staining; right: quantification of crypt height and Ki67+ cells. Scale bar, 50 μm. Vertical bars indicate the length of the crypts. Data are represented as mean ± SEM. ****P < 0.0001 (9 biological replicates, t-test).

E   RT–qPCR analysis of small intestines from Ythdf1^CTL and Ythdf1^cKO mice 72 h after 12 Gy IR. Data are represented as mean ± SEM. *P < 0.05, **P < 0.01 (5 biological replicates, t-test).

Source data are available online for this figure.

villus-enriched and crypt-enriched populations also revealed gradient expression of YTHDF1 from intestinal stem cell localized crypts to the differentiated villi (Fig 4B). Lineage tracing has identified the Wnt target gene leucine-rich repeat-containing G protein-coupled receptor 5 (LGR5) as an ISC marker [27]. Taken advantage of the *Lgr5-EGFP-IRES-creERT2* mouse, we examined the expression of YTHDF1 in epithelial cells with various degrees of stemness. The YTHDF1 expression level was high in the Lgr5-GFP^high stem cells, intermediate in the Lgr5-GFP^low transit-amplifying cell population, and low in the Lgr5-GFP^neg population (Fig 4C).

Given the high expression of YTHDF1 in ISCs, we asked whether *Ythdf1* deletion-induced intestinal defects are related to the dysfunction of ISCs. To this end, we deleted *Ythdf1* in Lgr5^+ ISCs using tamoxifen-inducible Lgr5-creERT (*Lgr5-creERT2:Ythdf1^{fl/fl}*) and performed organoid culture. *Ythdf1*-deficient organoids grew

comparably to the control organoids but only with less budding (Fig EV3A and B). Next, we cultured organoids with Wnt3a-conditioned medium. Wnt-treated organoids formed fast-growing "spheroids" displaying a cyst-like morphology lacking the budding crypts (Fig 4D and E). Surprisingly, *Ythdf1* deletion induced extensive budding by day 5, implying the loss of stemness (Fig 4D and E). Consistently, *Ythdf1* deletion in ISCs dramatically reduced the expression of stem cell markers Lgr5, Ascl2, and Olfm4, while increased the expression of differentiation markers ChgA, Anpep, and Fabp2 (Fig 4F).

To confirm that the observed defects resulted from loss of YTHDF1, we performed rescue experiments. We delivered lentivirus expressing either YTHDF1, YTH domain-deleted mutant, or a control vector (Fig EV3C). Re-expression of YTHDF1 in *Ythdf1*-deleted organoids substantially enhanced the spheroid features and restored the expressions of stem cell markers. However, the YTH domain-deleted
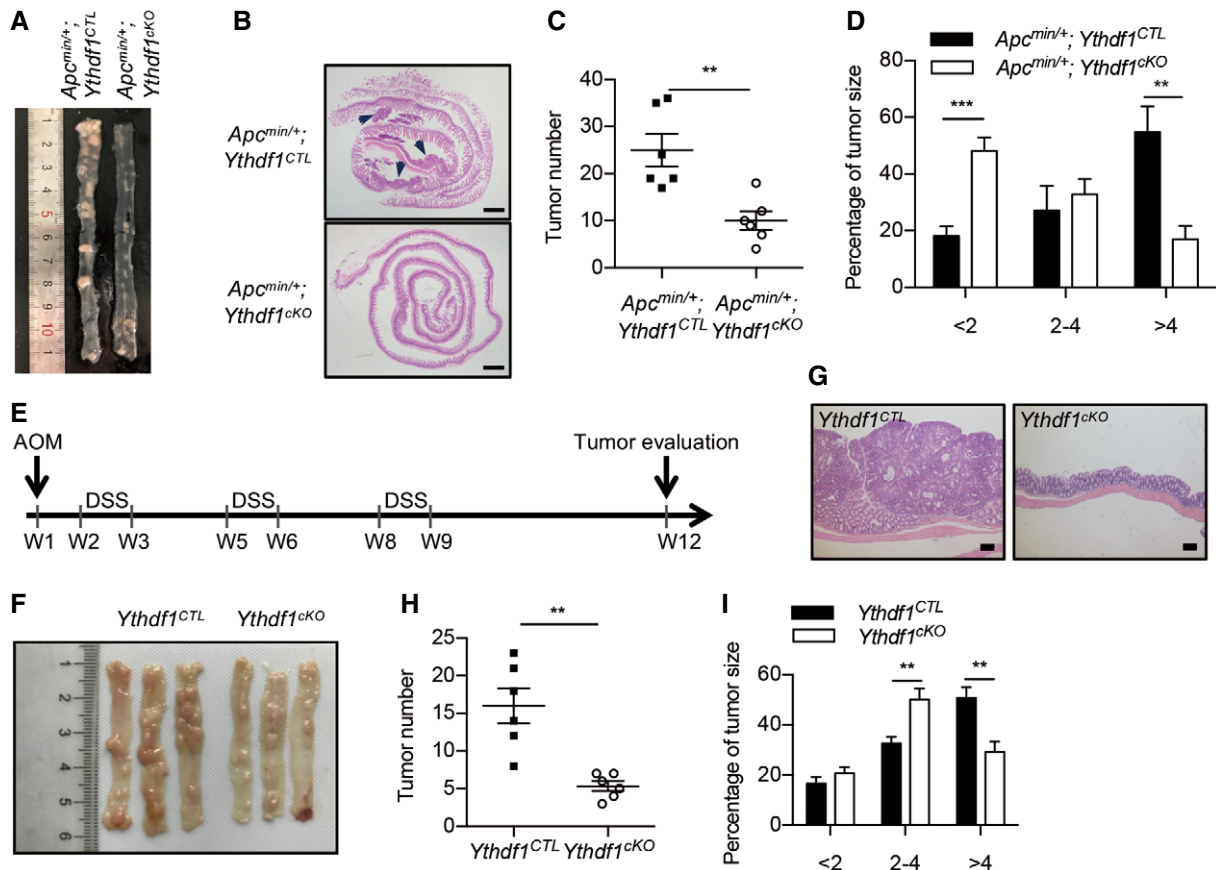
Figure 3. *Ythdf1* deletion reduces Wnt-driven tumorigenesis *in vivo*.

A   Small intestines from 24-week-old *Apc*$^{min/+}$; *Ythdf1*^{CTL} and *Apc*$^{min/+}$; *Ythdf1*^{cKO} mice.

B   H&E staining of small intestines from 24-week-old *Apc*$^{min/+}$; *Ythdf1*^{CTL} and *Apc*$^{min/+}$; *Ythdf1*^{cKO} mice. Scale bar, 1 mm. The black arrows indicate the tumors.

C, D Tumor number (C) and size distribution (D) from the small intestines of 24-week-old *Apc*$^{min/+}$; *Ythdf1*^{CTL} and *Apc*$^{min/+}$; *Ythdf1*^{cKO} mice. Data are shown as mean ± SEM (6 mice for each group). **$P < 0.01$, ***$P < 0.001$ (*t*-test).

E   Workflow of the AOM/DSS-induced colitis-associated cancer model.

F   Colons from *Ythdf1*^{CTL} and *Ythdf1*^{cKO} mice on day 84 of AOM/DSS induction.

G   H&E staining of colons from *Apc*$^{min/+}$; *Ythdf1*^{CTL} and *Apc*$^{min/+}$; *Ythdf1*^{cKO} mice after AOM/DSS induction. Scale bar, 200 μm.

H, I Colon tumor number (H) and size distribution (I) from *Ythdf1*^{CTL} and *Ythdf1*^{cKO} mice on day 84 of induction. Data are shown as mean ± SEM (6 mice for each group). **$P < 0.01$ (*t*-test).

YTHDF1 mutant could not rescue the phenotypes by *Ythdf1* deletion (Fig 4D–F). To substantiate the role of m^{6}A in the maintenance of stemness, METTL3 was silenced. Knockdown of METTL3 dramatically inhibited the growth of organoids and induced differentiation of organoids under Wnt3a treatment (Fig EV3D–G).

Transcriptome-wide identification of YTHDF1-regulated mRNAs

To identify potential targets regulated by YTHDF1, we performed antibody-based m^{6}A profiling and RNA sequencing (m^{6}A-seq) as well as RNA immunoprecipitation and sequencing (RIP-seq) in colorectal cancer cell line HCT116, harboring a constitutively activating mutation of β-catenin. m^{6}A-seq revealed the expected distribution of m^{6}A within the transcriptome and enrichment around the stop codon within transcripts (Fig EV4A). The analysis yielded 17,707 m^{6}A peaks within 8,076 transcripts (Fig EV4B and C, Dataset EV1). By combining with the RIP-seq data, we identified 3,388

m^{6}A-containing transcripts that are bound by YTHDF1 (referred to YTHDF1 targets, Fig EV4C and Dataset EV2). Given that YTHDF1 is known to affect mRNA translation [12], we assessed the changes in translational efficiency by ribosome profiling (Ribo-seq) after YTHDF1 knockdown using two shRNAs [12,28] (Fig EV4D and E, Dataset EV3). Data revealed 1015 decreased mRNAs and 387 increased mRNAs in translational efficiency after YTHDF1 knockdown, with slight changes in transcription (Fig 5A). As expected, we observed an elevated m^{6}A methylation level in the translational downregulated genes after YTHDF1 knockdown (Fig 5B). Reciprocally, we analyzed the translational changes based on m^{6}A modification. Data revealed a notable decrease in translational efficiency for m^{6}A-marked transcripts as well as YTHDF1 targets in YTHDF1 knockdown cells compared with control cells (Figs 5C and D, and EV4F and G).

To identify the functional pathways that are associated with YTHDF1-targeted mRNAs, we analyzed YTHDF1 targets that are
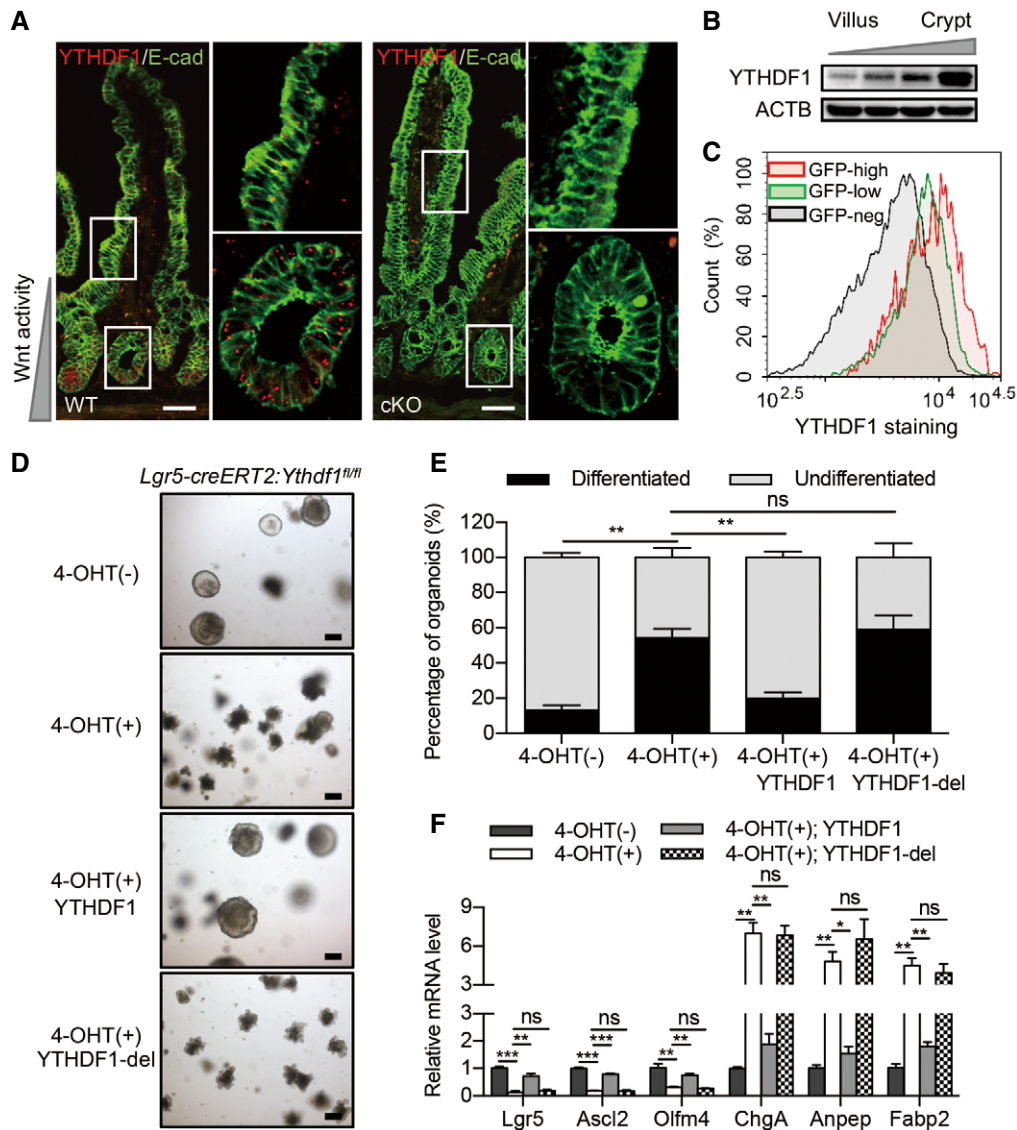
Figure 4. YTHDF1 is required for maintenance of intestinal stem cells.

A Fluorescent *in situ* hybridization for *Ythdf1* mRNA in *Ythdf1*^{CTL} and *Ythdf1*^{cKO} small intestines. Scale bar, 50 μm.
B Immunoblot analysis of fractionated murine intestine enriched for villus cells and crypt cells.
C Flow cytometry analysis of YTHDF1 protein expression in GFP$^{high/low/neg}$ populations from *Lgr5-GFP-IRES-creERT2* mice.
D Morphology of organoids from *Lgr5-creERT2:Ythdf1*$^{fl/fl}$ mice in Wnt3a-conditioned medium without or with 4-OHT induction and infected with lentivirus expressing YTHDF1 or YTHDF1 mutant. Scale bar, 250 μm.
E Quantification of differentiated versus undifferentiated organoids from (D). Data are represented as mean ± SEM. **$P < 0.01$ (4 biological replicates, *t*-test).
F Relative mRNA levels of intestinal stem cell and differentiation marker genes in organoids described in (D). Data are represented as mean ± SEM. 4 biological replicates. *$P < 0.05$, **$P < 0.01$, ***$P < 0.001$ (*t*-test).

Source data are available online for this figure.

translationally downregulated after YTHDF1 knockdown. Kyoto Encyclopedia of Genes and Genomes (KEGG) pathway enrichment analysis showed that the top enriched pathway was associated with the pluripotency of stem cells (Table EV1). Intriguingly, a subset of transcripts in this group were Wnt/β-catenin signaling components (Fig 5E and Table EV1), suggesting that Wnt signaling components are the main YTHDF1 targets during Wnt hyperactivation. qPCR analysis revealed that *LGR5* expression was dramatically reduced in

YTHDF1-silenced HCT116 cells (Fig EV4H). As *LGR5* is a direct target of β-catenin [24], our data indicated the reduced β-catenin activity after YTHDF1 knockdown.

TCF7L2/TCF4 is a key functional target of YTHDF1

Focusing on the potential candidates implicated in Wnt signaling, we noticed that T-cell factor 7-like 2/T-cell factor 4 (TCF7L2/TCF4)
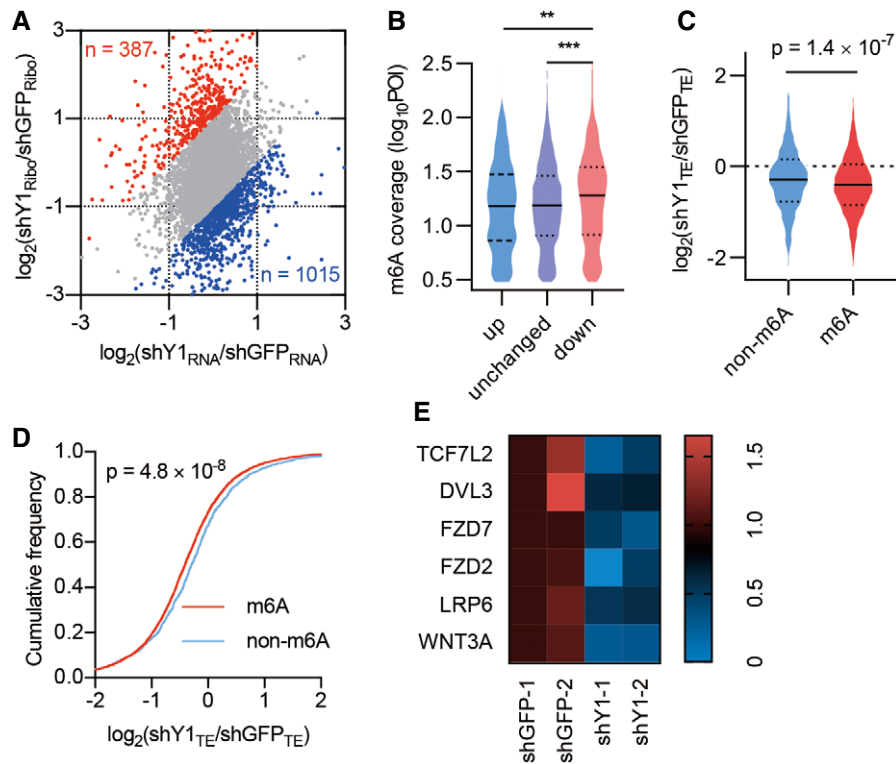
Figure 5. Transcriptome-wide identification of YTHDF1-regulated mRNAs.

A   Scatterplot of mRNA expression and ribosome profiling data from control and YTHDF1 knockdown cells. The upregulated (red) and downregulated (blue) genes in translational efficiency (TE) are highlighted.

B   The relative m6A peak coverage in control cells for transcripts grouped according to TE changes after YTHDF1 knockdown. POI: peak over input. Down, genes significantly downregulated in YTHDF1 knockdown cells (< 0.5 fold). Unchanged, genes not significantly changed. Up, genes significantly upregulated (> 2 fold). The upper and lower quartiles and the median are shown for each group. Mann–Whitney test. **$P < 0.01$. ***$P < 0.001$.

C   Violin plots showing TE change between control and YTHDF1 knockdown cells for non-methylated (non-m6A) and methylated (m6A) transcripts. The upper and lower quartiles and the median are indicated for each group. Mann–Whitney test.

D   Cumulative distributions of TE change for non-m6A and m6A transcripts as in (C). Kolmogorov–Smirnov test.

E   Heatmap showing the TE of Wnt signaling components in control and YTHDF1 knockdown cells. The values show the fold change of the indicated color of the heatmap.

was listed as the top candidate, showing reduced translation upon YTHDF1 deletion (Figs 5E and EV4I). TCF7L2 belongs to the LEF/TCF family, which are the key nuclear effectors of the canonical β-catenin transcription. YTHDF1 knockdown in HCT116 cells dramatically reduced the protein level but not the mRNA level of TCF7L2 (Figs 6A and EV5A). Polysome profiling revealed reduced translation of TCF7L2 in YTHDF1-silencing cells (Fig 6B). In addition, inhibited expression of TCF7L2 was also observed in the Ythdf1-depleted crypt (Figs 6C and EV5B). Next, we investigated the regulation of TCF7L2 by YTHDF1 through m6A in the 3′UTR using luciferase assay. Erasing m6A by silencing METTL3 decreased luciferase activity, suggesting the involvement of m6A in TCF7L2 3′UTR translation (Fig EV5C). YTHDF1 knockdown decreased luciferase activity, suggesting that YTHDF1 mediates the translation of TCF7L2 3′UTR (Fig EV5D). Collectively, these results indicated that the translation of TCF7L2 is directly regulated by YTHDF1.

Next, we asked whether YTHDF1-mediated TCF7L2 translation is regulated by Wnt signaling. Indeed, Wnt3a treatment dramatically promoted the translation of TCF7L2, as revealed by

immunoblot and polysome profiling (Figs 6D and EV5E). Methylated RNA immunoprecipitation showed increased m6A levels on TCF7L2 in Wnt3a-treated crypt (Fig 6E). In agreement, RNA immunoprecipitation demonstrated that Wnt3a treatment increased the binding between YTHDF1 and TCF7L2 mRNA (Fig 6F). Together, these results indicated that Wnt signaling regulates the translation of TCF7L2 in an m6A-dependent manner.

Finally, we asked whether the deficient translation of TCF7L2 could explain the disrupted Wnt signaling in the absence of YTHDF1. As such, β-catenin-driven transcription activity was measured by the TOP[Flash]/FOP[Flash] luciferase reporter assay. Indeed, overexpression of TCF7L2 rescued the decreased β-catenin activity in YTHDF1 knockdown cells (Fig 6G). To ascertain the contribution of TCF7L2 in YTHDF1-mediated intestinal stem cell maintenance, we performed rescue experiments in Wnt3a-treated organoids. As reflected by the undifferentiated organoid percentage, overexpression of TCF7L2 reversed the stemness loss elicited by Ythdf1 deletion (Fig 6H and I). Collectively, our results indicated that YTHDF1 deletion reduces the
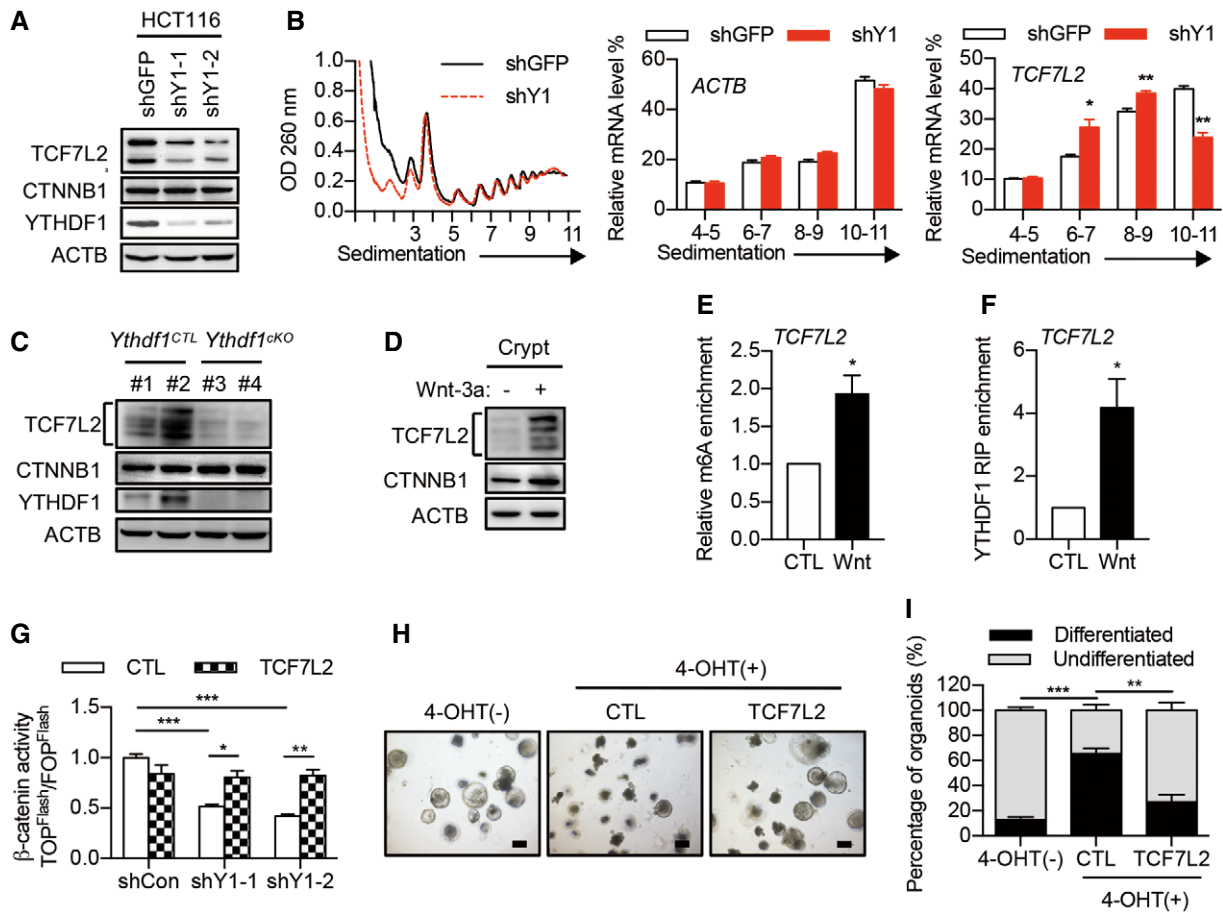
Figure 6. TCF7L2 is a key functional target of YTHDF1.

A   Immunoblot analysis of HCT116 cells with YTHDF1 knockdown. Two major bands were detected for human TCF7L2 due to alternative splicing.
B   Polysome profiles of HCT116 cells with or without YTHDF1 knockdown. The right panels show the distributions of *TCF7L2* and *ACTB* in polysome fractions. Data are represented as mean ± SEM. *$P < 0.05$, **$P < 0.01$ (3 biological replicates, *t*-test).
C   Immunoblot analysis of crypts from *Ythdf1^CTL* and *Ythdf1^cKO* mice. Multiple bands were detected for mouse TCF7L2 representing different isoforms.
D   Immunoblot analysis of mouse intestinal crypts treated with Wnt3a for 60 min.
E   MeRIP-qPCR analysis of m⁶A levels of *TCF7L2* in crypts treated with or without Wnt3a. Data are represented as mean ± SEM. *$P < 0.05$ (3 biological replicates, *t*-test).
F   RIP analysis of the interaction of YTHDF1 with *TCF7L2* mRNA. The enrichment was measured by qPCR and normalized to input. Data are represented as mean ± SEM. *$P < 0.05$ (3 biological replicates, *t*-test).
G   β-catenin/TCF4 reporter activity in YTHDF1 knockdown cells infected with lentivirus expressing TCF7L2. Data are represented as mean ± SEM. *$P < 0.05$, **$P < 0.01$, ***$P < 0.001$ (3 biological replicates, *t*-test).
H   Morphology of organoids from *Lgr5-creERT2:Ythdf1^fl/fl* mice in Wnt3a-conditioned medium without or with 4-OHT induction and infected with lentivirus expressing TCF7L2. Scale bar, 250 μm.
I   Quantification of differentiated versus undifferentiated organoids from (H). Data are represented as mean ± SEM. **$P < 0.01$, ***$P < 0.001$ (3 biological replicates, *t*-test).

Source data are available online for this figure.

translation of *TCF7L2*, leading to the inactivation of Wnt signaling and loss of stemness.

Targeting YTHDF1 in ISCs of established tumors leads to tumor shrinkage and prolonged survival

YTHDF1 is dispensable for physiological intestinal development but is essential for tumorigenesis, making it an ideal potential target for CRC treatment. We, therefore, depleted *Ythdf1* in ISCs after AOM/DSS or *Apc* mutation-induced tumor formation using the tamoxifen-inducible *Lgr5-creERT2* line (Fig 7A and E). We observed tumor formation in normal mice after 6 weeks of AOM/ DSS treatment or *Apc^{min/+}* mice after 3 months of high-fat diet (Fig EV5F and G). Successful *Ythdf1* depletion in the intestinal epithelial cells was confirmed by immunoblot (Fig EV5H and I). *Ythdf1* deletion dramatically reduced both tumor number and tumor load in AOM/DSS-induced tumors (Fig 7B and C). Moreover, the expression of TCF7L2, FZD7, and MYC was decreased in tumors from *Ythdf1* knockout mice compared with WT mice (Fig 7D). Kaplan–Meier survival plots revealed that the life span
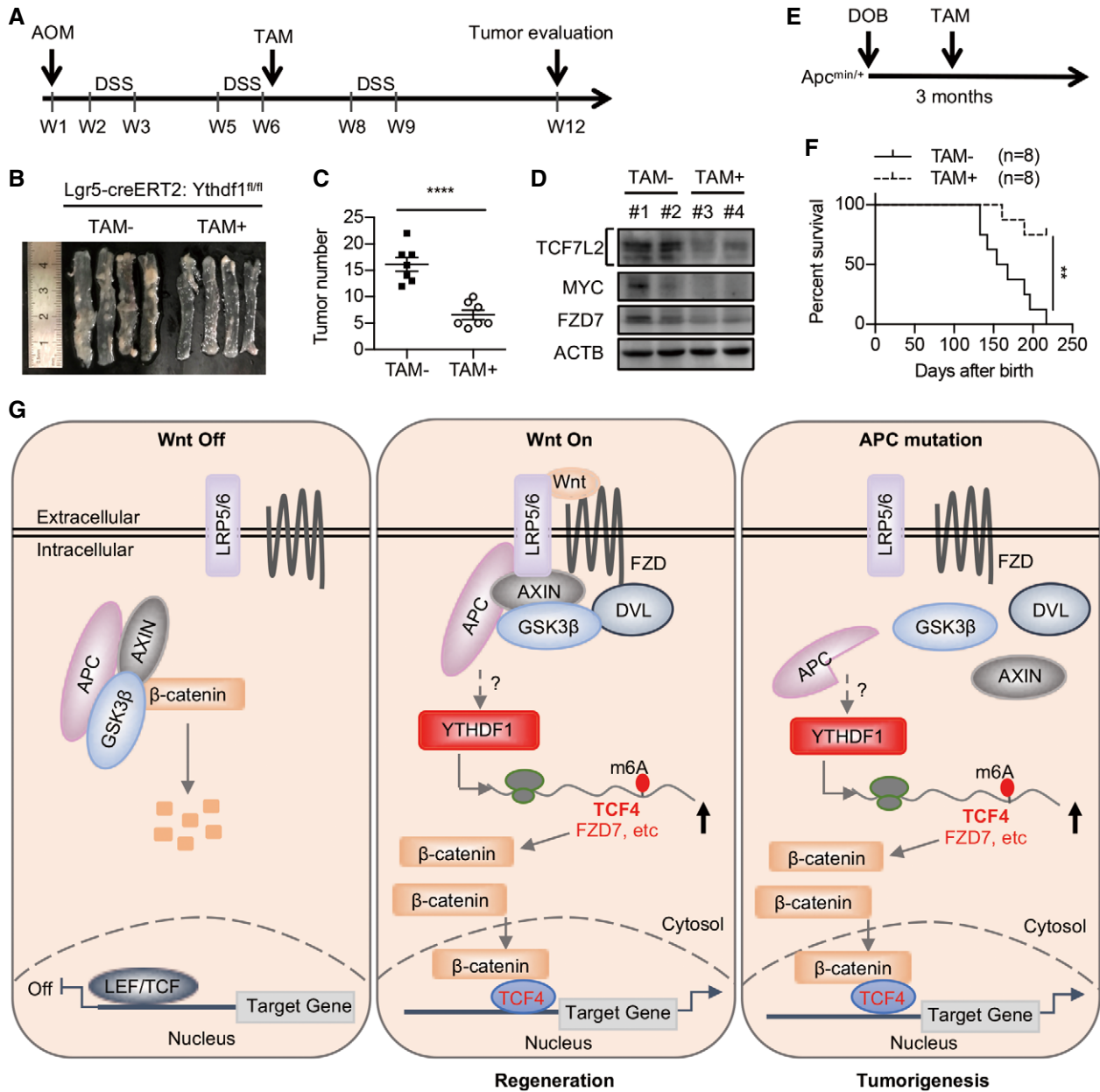
Figure 7. Targeting YTHDF1 in ISCs of established tumors leads to tumor shrinkage and prolonged survival.

A   Workflow of tamoxifen (TAM)-induced *Ythdf1* deletion in AOM/DSS-induced *Lgr5-creERT2:Ythdf1^fl/fl^* mice.
B   Colons from mice in (A) treated with or without TAM on day 80 of AOM/DSS induction.
C   Colon tumor number from mice treated with or without TAM on day 80 of AOM/DSS induction. Data are shown as mean ± SEM (7 mice for each group).
    ****$P < 0.0001$ (*t*-test).
D   Immunoblot analysis of 2 pairs of colon tumors from mice treated with or without TAM.
E   Workflow of tamoxifen (TAM)-induced *Ythdf1* deletion in *Apc^min/+^* mice.
F   Kaplan–Meier survival plots for *Apc^min/+^*; *Lgr5-creERT2:Ythdf1^fl/fl^* mice (8 mice for each group) treated with or without TAM. Log-rank (Mantel–Cox) test. **$P < 0.01$ (*t*-test).
G   A proposed model of amplified β-catenin activity by m6A-YTHDF1-mediated translation.

Source data are available online for this figure.

was much longer in *Ythdf1*-deleted *Apc^min/+^* mice (Fig 7F). Together, these results demonstrated that YTHDF1 inhibition indeed has the therapeutic benefit. Additionally, these results further supported the notion that YTHDF1 in ISCs plays a major role during CRC development.

Discussion

It has generally been accepted that Wnt/β-catenin signaling drives the self-renewal of ISCs, which is essential for intestinal homeostasis, regeneration, and tumorigenesis. Due to its critical role, the activity

of β-catenin is under the control of several highly regulated processes, including ligand–receptor interactions, β-catenin stability, β-catenin nuclear translocation, and β-catenin transcriptional activity. Here, we report an additional checkpoint for β-catenin activation that involves m6A modification-dependent and YTHDF1-mediated translation of β-catenin mediator TCF7L2/TCF4. The coordination between β-catenin stabilization and translational induction of TCF7L2 promotes the final production of β-catenin targets, which is co-opted by ISCs to maintain their stemness (Fig 7G).

The biological function of m6A is regulated at multiple layers by the methyltransferases, demethylases, and reader proteins [29]. The impact of m6A modification in stem cell biology is still complex due to the context-dependent function of the "writers", "erasers", and "readers" [16–20]. Taken advantage of the conditional knockout mice model and cultured organoids, we demonstrated that YTHDF1 is required for the maintenance of ISC features during Wnt-driven intestinal regeneration and tumorigenesis. The function of YTHDF1 relies on its m6A-binding activity as wild-type YTHDF1 rescues the phenotype of *Ythdf1^cKO* organoid growth while an m6A-binding domain-deleted mutant cannot. Moreover, knockdown of METTL3 inhibits organoid growth, highlighting an essential role of m6A in the maintenance of intestinal stem cells. Intriguingly, our study strongly indicated that the function of YTHDF1 relies on Wnt activation, as YTHDF1 is dispensable for normal intestinal development. It should be noted that whole-body *Ythdf1* knockout mice are viable but have learning and memory defects [30], further indicating the context-dependent function of YTHDF1. Taken together, our findings supported the notion that YTHDF1 is the major effector of m6A in the intestines to maintain stem cell traits during regeneration and tumorigenesis.

In agreement with the previous reports that YTHDF1 is a translation regulator [12,30,31], our data demonstrated that YTHDF1 exerts its function through regulating the translation of a subset of mRNAs. By combining RIP-seq, m6A-seq, and Ribo-seq, we have identified *TCF4*, *DVL3*, and *FZD7* as the direct targets of YTHDF1, three key Wnt signaling components. Importantly, our rescue experiments have confirmed TCF7L2 as a key functional target of YTHDF1. As the major transcriptional effector for β-catenin in mouse intestine and human colorectal cancer cells, TCF7L2 is essential for both intestinal homeostasis and tumorigenesis [32]. In our study, expression of TCF7L2 largely rescues the reduced β-catenin activity and stem cell features by YTHDF1 deletion, emphasizing the importance of this protein for intestinal stem cell maintenance. Among the ten mammalian FZD receptors, FZD7 is enriched in Lgr5+ stem cells and functions as the major FZD receptor responsible for mediating Wnt activity in intestinal stem cells [33]. In addition, FZD7 was reported to control intestinal regeneration via MYC [33]. Indeed, as a direct Wnt target, MYC is critical for intestinal regeneration [34]. Our data clearly demonstrated that knockout of *Ythdf1* reduces the expression of FZD7 and MYC in both irradiation model and AOM/DSS model, highlighting the essential role of YTHDF1-promoted expression of these factors in Wnt-driven regeneration and tumorigenesis. Of note, our Ribo-seq data showed that the translation of β-catenin did not change. However, the protein level of β-catenin decreased in *Ythdf1*-deleted crypt under Wnt treatment. This might be due to the degradation of β-catenin, as FZD7 and DVL3 are regulators of β-catenin protein stability.

Studies have shown that YTHDF1 regulates translation in a stimulation-induced manner [35]. For instance, in the dorsal root ganglion (DRG) model of injury-induced axon regeneration, YTHDF1 is required for robust global *de novo* protein synthesis only during this recovery process but has little effect on translation before the injury [36]. Another study showed that YTHDF1-dependent translation was enhanced only by potassium chloride depolarization in cultured neurons [30]. In line with these reports, we found that YTHDF1-mediated translation of *TCF7L2* largely depends on Wnt activation. Based on our data, Wnt signaling triggers YTHDF1-mediated translation through two coordinated aspects. On the one hand, Wnt increases m6A methylation on *TCF7L2* (cis-element), due to the upregulated expression of METTL3 (Fig 1A). On the other hand, Wnt promotes the expression of YTHDF1 (trans-factor). These results account for the Wnt-dependent phenotype of YTHDF1 observed in mice at the molecular level.

YTHDF1 upregulation is consistently observed in human and mouse intestinal cancer (Figs 1G and EV1I–L) [37,38], making this protein a robust and reproducible biomarker for CRC. The expression of YTHDF1 is regulated at multiple levels. Both upregulated transcription and amplified DNA copy number might contribute to the high expression of YTHDF1 in CRC [37,38]. This is supported by the upregulated *YTHDF1* mRNA level in TCGA datasets (Fig EV1L). Mutations in *APC* gene are observed in more than 80% of CRC patient samples [5,22], prompting the search for vulnerabilities specific to *APC* mutation. Using *in vitro* and *in vivo* models, we defined that *APC* mutation induces YTHDF1 expression mainly at the translational level, which provides an additional layer of YTHDF1 expression regulation. Our data indicated that YTHDF1 expression is regulated by Wnt and APC but not β-catenin. This could be explained by the fact that Wnt/APC could regulate gene expression independent of β-catenin. For instance, Wnt was reported to regulate mRNA translation through mTOR [39]. Moreover, APC could regulate the activity of transcription factor YAP, potentially regulating gene expression [40]. The mechanism of Wnt/APC-regulated YTHDF1 expression needs further investigation.

YTHDF1 is dispensable for physiological intestinal development while essential for Wnt-driven tumorigenesis, making it an ideal therapeutic target for CRC. Indeed, our mouse data demonstrated that deletion of *Ythdf1* in the established tumors using genetic methods leads to tumor shrinkage and prolonged survival. Of note, a recent study has demonstrated that YTHDF1 regulates durable neoantigen-specific immunity. Loss of YTHDF1 in classical dendritic cells enhanced cross-presentation of tumor antigens and the cross-priming of CD8+ T cells, implicating YTHDF1 as a potential therapeutic target in anticancer immunotherapy [31]. We envision that compounds targeting YTHDF1 may increase the efficacy of the current CRC therapy regime by inhibiting cancer stem cell activity as well as increasing anticancer immune response.

In summary, our findings highlighted an essential role of YTHDF1 in Wnt signaling activation, intestinal stem cell trait maintenance, and CRC, with potential implications for disease intervention. In addition, our results established a model for m6A-dependent and YTHDF1-mediated translation in signaling amplification, which may guide the understanding of the development and progression of other human disorders associated with m6A/YTHDF1 dysregulation.

Materials and Methods

Mouse experiments

Mice were maintained and bred in specific pathogen-free conditions at the Animal Center of Zhejiang University. All animal studies were performed in compliance with the Guide for the Care and Use of Laboratory Animals by the Medical Experimental Animal Care Commission of Zhejiang University. All animal studies used the protocol that has been approved by the Medical Experimental Animal Care Commission of Zhejiang University. For each experiment, about 6–10 mice were used for each group. Randomization and blinding were used for animal studies.

Conditional *Ythdf1* KO allele (*Ythdf1$^{fl/fl}$*) was generated at C57BL/6 strain by Cyagen Biosciences (China). The fourth exon of *Ythdf1* was targeted with flanking LoxP sites. *Villin-Cre, Lgr5-EGFP-IRES-creERT2*, and *Apc$^{min/+}$* mice were obtained from the Jackson Laboratory.

Irradiation injury

For irradiation, 2-month-old mice were subjected to 12 Gy gamma irradiation in a Rad Source (RS2000Pro, Rad Source Technologies) and executed at the appointed time.

Apc$^{min/+}$ spontaneous mouse tumor model

For the detection of *Apc* mutation-induced tumorigenesis, *Apc$^{min/+}$* mice were allowed to develop tumors spontaneously for 6 months and then sacrificed for tumor and tissue analysis. For survival analysis, *Apc$^{min/+}$; Lgr5-EGFP-IRES-creERT2:Ythdf1$^{fl/fl}$* mice were fed with a high-fat diet. At the age of 3 months, mice were injected intraperitoneally with tamoxifen at 2 mg/day for 5 days to induce *Ythdf1* deletion and survival is monitored.

The AOM/DSS-induced mouse colorectal cancer model

Two-month-old female *Ythdf1$^{fl/fl}$* (*Ythdf1^{CTL}*) and *Villin-Cre:Ythdf1$^{fl/fl}$* (*Ythdf1^{cKO}*) littermates were intraperitoneally injected once with AOM (Sigma) at 10 mg/kg body weight. One week after AOM injection, mice were subjected to DSS cycle, in which mice were fed with 2.5% (w/v) DSS (molecular weight 36,000–50,000, MP Biomedicals) for 7 days followed by 14 days of normal water feeding. After three cycles of DSS treatment, mice were sacrificed on week 12 and colon tissues were collected for tumor number and volume evaluation. To investigate the effect of *Ythdf1* deletion in intestinal stem cells on tumor development, *Lgr5-EGFP-IRES-creERT2:Ythdf1$^{fl/fl}$* mice were subjected to AOM/DSS treatment. In the second cycle of DSS treatment, mice were injected intraperitoneally with tamoxifen at 2 mg/day for 5 days to induce *Ythdf1* deletion.

Histology and immunohistochemistry

Intestines were rinsed with DPBS, fixed in 10% formalin, paraffin-embedded, and sectioned at 5 mm. Sections were stained with hematoxylin and eosin (H&E). For immunohistochemistry, antigen retrieval was performed by heating slides in 0.01 M citrate buffer (pH 6.0) in a microwave. Antibodies used for immunohistochemistry are listed in Table EV2. Diaminobenzidine (DAB) was used as the enzyme substrate for staining, and hematoxylin was used as the counterstain.

RNA fluorescent *in situ* hybridization (FISH)

Mouse intestinal tissue was excised and fixed in 4% paraformaldehyde for 24 h at 4°C. Fixed tissues were dehydrated in a graded series of sucrose and embedded in OCT compound (Sakura Finetek) and frozen on dry ice. Cryostat sections (7 μm) were cut and dried for 20 min. RNA fluorescent *in situ* hybridization was then performed according to the RNAScope Multiplex Fluorescent Assay (ACD, Inc) following the manufacturer's protocol.

Plasmid construction

Flag-tagged YTHDF1 was generated from HEK293T cell line cDNA and cloned into vector pCDH-CMV-MCS-EF1-Puro at EcoRI/BamHI. Flag-tagged TCF7L2 was generated from HCT116 cell line cDNA and cloned into vector pCDH-CMV-MCS-EF1-Puro using recombinational cloning kit (Vazyme, China). YTHDF1-5′UTR was generated from HCT116 cell line cDNA and cloned into vector pGL3-control (Promega) at HindIII/NcoI. The primers used for the cloning are listed in Table EV3.

For shRNA knockdown experiments, specific shRNA oligos (Table EV3) were annealed and cloned to the lentiviral vector pLKO.1.

Crypt isolation, treatment, and culture

Small intestinal crypt from normal intestinal tissues and adenoma were isolated using EDTA as described previously [41,42]. The isolated crypts resuspended in DMEM/F12 (Invitrogen) were treated with or without Wnt3a (60 ng/ml) for 30 or 60 min. The crypts were then subjected to further analysis. For organoid culture, crypts were embedded in Matrigel (BD) and cultured in advanced DMEM/F12 (Invitrogen) supplemented with 2 mM GlutaMAX (Invitrogen), penicillin/streptomycin, 1 μM N-acetyl cysteine (Sigma), 1×B27 supplement (Invitrogen), 1×N2 supplement (Invitrogen), 50 ng/ml EGF (PeproTech), 100 ng/ml Noggin (PeproTech), and 500 ng/ml R-spondin (PeproTech).

Human colorectal cancer tissue samples

The colorectal cancer tissue arrays were purchased from Shanghai Outdo Biotech Company (OD-CT-DgCol01-006 and HcolA030PG06). Ethical consent was granted from the Ethical Committee Review Board of Shanghai Outdo Biotech Company. The informed consent was obtained from all subjects and that the experiments conformed to the principles set out in the WMA Declaration of Helsinki and the Department of Health and Human Services Belmont Report.

Cell culture

Human colorectal cancer cell lines SW620, HCT116, and RKO are obtained from ATCC and cultured in DMEM (HyClone) supplemented with 10% fetal bovine serum (Thermo Fisher Scientific). Cells were maintained at 37°C in an atmosphere containing 5% CO_2.

Quantitative RT–PCR

Total RNA was isolated from total mouse small intestinal epithelial cells using TRIzol reagent (Life Technologies). Each RNA sample was reverse-transcribed with the M-MLV Reverse Transcriptase (Takara) using random primers. Real-time PCR was performed using the SYBR Green I Master Mix on a LightCycler 480 Real-Time PCR System (Roche). Relative gene expression was normalized to the expression of ACTB or GAPDH and was calculated using the $2^{(-\Delta\Delta CT)}$ method. RT–qPCR primers are listed in Table EV3.

Immunoblotting

Cells or intestinal epithelial tissues were lysed in RIPA lysis buffer (Beyotime, China). 40 μg of total protein was separated by sodium dodecyl sulfate–polyacrylamide gel (SDS–PAGE) under denaturing conditions and transferred to PVDF membranes (Millipore). Membranes were blocked in 5% non-fat dry milk in TBST and incubated with primary antibodies, followed by incubation with the secondary antibody and chemiluminescent detection system (Bio-Rad). The primary antibodies used are listed in Table EV2.

Polysome profiling

SW620 cells or HCT116 cells were treated with cycloheximide (CHX) at 100 μg/ml for 3 min to freeze the translating ribosomes. Cells were pelleted, lysed with lysis buffer (10 mM HEPES, pH 7.4, 100 mM KCl, 5 mM $MgCl_2$, 100 μg/ml CHX, 5 mM DTT, and 1% Triton X-100) on ice, and centrifuged. The supernatant was collected and loaded onto a 10–50% w/v sucrose gradient prepared in the polysome buffer (10 mM HEPES, pH 7.4, 100 mM KCl, 5 mM $MgCl_2$, and 100 μg/ml CHX). The gradients were centrifuged at 4°C for 2.5 h at 178,305 *g* (Beckman, rotor SW41Ti). The sample was then fractioned by Gradient Station (BioCamp) equipped with a UV monitor and collected with a fraction collector (FC203B, Gilson). Total RNA from the indicated fractions was isolated by TRIzol reagent for RT–qPCR analysis.

Luciferase reporter assay

To study the regulation of β-catenin activity by YTHDF1, SW620 cells infected with shYTHDF1 virus were co-transfected with TOP[Flash] or FOP[Flash] firefly luciferase reporter plasmid and Renilla luciferase reporter (Promega) as an internal control. Cells were harvested at 24 h post-transfection. Firefly and Renilla luciferase activities were measured using the Dual-Luciferase Assay Kit (Promega). The activities of the TOP[Flash] and the FOP[Flash] reporter constructs were expressed as normalized relative light units to the Renilla internal control. For β-catenin/TCF-4 induction experiments, results were presented as fold induction. Fold induction was determined by normalizing TOP[Flash] value to FOP[Flash] value.

To study the regulation of YTHDF1 5′UTR translation, SW620 cells with or without APC expression were transfected with YTHDF1-5′UTR-Luc construct together with Renilla luciferase reporter. Firefly and Renilla luciferase activities were measured using the Dual-Luciferase Assay Kit (Promega). Firefly luciferase activity was normalized by Renilla luciferase activity.

To study the regulation of TCF7L2 3′UTR translation, HCT116 cells with or without APC expression were transfected with Luc-TCF7L2-3′UTR construct together with Renilla luciferase reporter. Firefly and Renilla luciferase activities were measured using the Dual-Luciferase Assay Kit (Promega). Firefly luciferase activity was normalized by Renilla luciferase activity.

m⁶A RIP qPCR

Total RNA was isolated from SW620 cells using TRIzol, and polyadenylated RNA was further enriched using the Dynabeads Oligo(dT)$_{25}$ (Invitrogen). Dynabeads™ Protein G beads (Invitrogen) were coated with 3 μg m⁶A antibody (Synaptic Systems) and washed 2 times with 1×IP buffer (10 mM Tris–HCl pH 7.6, 150 mM NaCl, 0.1% Igepal CA-630, and 200 U/ml RNase inhibitor). Purified mRNA was then incubated with m⁶A-coated beads for 6 h at 4°C. The beads were washed three times with 1 ml ice-cold washing buffer (10 mM Tris–HCl pH 7.6, 0.15 M LiCl, and 1 mM EDTA). The immunoprecipitation complex was digested with proteinase K at 55°C for 1 h. RNA was then extracted using TRIzol reagent (Life Technologies), followed by quantitative RT–PCR.

RNA-seq

Total RNA was isolated from control cells or YTHDF1 knockdown cells using TRIzol reagent. Polyadenylated RNA was further enriched from total RNA using the Dynabeads Oligo(dT)$_{25}$ (Invitrogen). mRNA samples were fragmented into ~100-nucleotide-long fragments using RNA Fragmentation Reagents (Ambion, AM8740) and used for library construction and high-throughput sequencing. The sequencing was performed by Hangzhou KaiTai Biotechnology Co., Ltd.

m⁶A-seq

Dynabeads™ Protein G beads (Invitrogen) were coated with 5 μg anti-m⁶A antibody in 1×IP buffer (10 mM Tris–HCl, pH 7.4, 150 mM NaCl, and 0.1% NP-40) for 0.5 h. 3 μg of fragmented mRNA was incubated with antibody-coated Protein G beads at 4°C for 4 h. After washing three times with IP buffer, bound RNA was eluted using 100 μl elution buffer (6.7 mM N6-methyladenosine 5′-monophosphate sodium salt in 1×IP buffer), followed by ethanol precipitation. Precipitated RNA was used for library construction and high-throughput sequencing.

Ribo-seq

Control cells or YTHDF1 knockdown cells were treated with CHX (100 μg/ml) for 3 min at 37°C to freeze the translating ribosomes. Cells were then harvested by polysome lysis buffer (10 mM HEPES, pH 7.4, 100 mM KCl, 5 mM $MgCl_2$, 100 μg/ml CHX, 5 mM DTT, and 1% Triton X-100). After centrifugation at 4°C and 12,000× *g* for 10 min, the supernatant was digested with *E. coli* RNase I (Ambion) at 4°C for 1 h. Ribosome-protected fragments were collected by centrifugation for 134 min at 449,165 *g* using an MLA150 rotor in 1 M sucrose cushion. Total RNA was extracted using TRIzol reagent. The end structures of the RNA fragments of ribosome profiling were repaired by T4 PNK as described previously [11]. The

library was constructed by TruSeq Small RNA Sample Preparation Kit (Illumina).

Sequencing data analysis

The 3′ adaptors and low-quality bases were trimmed by Cutadapt3. The trimmed reads with length < 15 nucleotides were excluded. The remaining reads were mapped to the human transcriptome using Bowtie. For read alignment, a maximum of two mismatches was permitted. m⁶A coverages at individual sites were normalized by the mean coverage of the transcript. For Ribo-seq, the reads mapped to CDS were used to calculate the RPKM values for translation levels. For RNA-seq, the reads mapped to the entire transcript were used to calculate RPKM. Translational efficiency (TE) was defined as the ratio of FPKM of Ribo-seq over FPKM of RNA-seq.

Statistical analysis

Statistical analysis was performed using GraphPad Prism 9 software (GraphPad Software, Inc.). P values were calculated using a two-tailed t-test unless stated otherwise. Asterisks denote statistical significance (*$P < 0.05$; **$P < 0.01$; ***$P < 0.001$).

Data availability

The datasets produced in this study are available in the following databases: m6A-seq, Ribo-seq, and RNA-seq data: Gene Expression Omnibus GSE136664 (https://www.ncbi.nlm.nih.gov/geo/query/acc.cgi?acc = GSE136664).

Expanded View for this article is available online.

Author contributions

BH, SW, and SY performed the majority of experiments. JX assisted with the molecular experiments. KL performed the analysis. ZC, RB, and JS assisted with the mice experiments. ZX and XG designed the experiments. XG conceived the project and wrote the manuscript. All authors discussed the results and edited the manuscript.

Conflict of interest

The authors declare that they have no conflict of interest.

References

1. Barker N (2014) Adult intestinal stem cells: critical drivers of epithelial homeostasis and regeneration. *Nat Rev Mol Cell Biol* 15: 19–33

2. Nusse R, Clevers H (2017) Wnt/beta-catenin signaling, disease, and emerging therapeutic modalities. *Cell* 169: 985–999

3. Miyoshi H, Ajima R, Luo CT, Yamaguchi TP, Stappenbeck TS (2012) Wnt5a potentiates TGF-beta signaling to promote colonic crypt regeneration after tissue injury. *Science* 338: 108–113

4. Morin PJ, Sparks AB, Korinek V, Barker N, Clevers H, Vogelstein B, Kinzler KW (1997) Activation of beta-catenin-Tcf signaling in colon cancer by mutations in beta-catenin or APC. *Science* 275: 1787–1790

5. Korinek V, Barker N, Morin PJ, van Wichen D, de Weger R, Kinzler KW, Vogelstein B, Clevers H (1997) Constitutive transcriptional activation by a beta-catenin-Tcf complex in APC-/- colon carcinoma. *Science* 275: 1784–1787

6. Bokar JA, Shambaugh ME, Polayes D, Matera AG, Rottman FM (1997) Purification and cDNA cloning of the AdoMet-binding subunit of the human mRNA (N6-adenosine)-methyltransferase. *RNA* 3: 1233–1247

7. Liu J, Yue Y, Han D, Wang X, Fu Y, Zhang L, Jia G, Yu M, Lu Z, Deng X *et al* (2014) A METTL3-METTL14 complex mediates mammalian nuclear RNA N6-adenosine methylation. *Nat Chem Biol* 10: 93–95

8. Ping XL, Sun BF, Wang L, Xiao W, Yang X, Wang WJ, Adhikari S, Shi Y, Lv Y, Chen YS *et al* (2014) Mammalian WTAP is a regulatory subunit of the RNA N6-methyladenosine methyltransferase. *Cell Res* 24: 177–189

9. Jia G, Fu Y, Zhao X, Dai Q, Zheng G, Yang Y, Yi C, Lindahl T, Pan T, Yang YG *et al* (2011) N6-methyladenosine in nuclear RNA is a major substrate of the obesity-associated FTO. *Nat Chem Biol* 7: 885–887

10. Zheng G, Dahl JA, Niu Y, Fedorcsak P, Huang CM, Li CJ, Vagbo CB, Shi Y, Wang WL, Song SH *et al* (2013) ALKBH5 is a mammalian RNA demethylase that impacts RNA metabolism and mouse fertility. *Mol Cell* 49: 18–29

11. Wang X, Lu Z, Gomez A, Hon GC, Yue Y, Han D, Fu Y, Parisien M, Dai Q, Jia G *et al* (2014) N6-methyladenosine-dependent regulation of messenger RNA stability. *Nature* 505: 117–120

12. Wang X, Zhao BS, Roundtree IA, Lu Z, Han D, Ma H, Weng X, Chen K, Shi H, He C (2015) N(6)-methyladenosine modulates messenger RNA translation efficiency. *Cell* 161: 1388–1399

13. Zhou J, Wan J, Gao X, Zhang X, Jaffrey SR, Qian SB (2015) Dynamic m(6)A mRNA methylation directs translational control of heat shock response. *Nature* 526: 591–594

14. Meyer KD, Patil DP, Zhou J, Zinoviev A, Skabkin MA, Elemento O, Pestova TV, Qian SB, Jaffrey SR (2015) 5′ UTR m(6)A promotes cap-independent translation. *Cell* 163: 999–1010

15. Zhao BS, Roundtree IA, He C (2017) Post-transcriptional gene regulation by mRNA modifications. *Nat Rev Mol Cell Biol* 18: 31–42

16. Geula S, Moshitch-Moshkovitz S, Dominissini D, Mansour AA, Kol N, Salmon-Divon M, Hershkovitz V, Peer E, Mor N, Manor YS *et al* (2015) Stem cells m6A mRNA methylation facilitates resolution of naive pluripotency toward differentiation. *Science* 347: 1002–1006

17. Batista PJ, Molinie B, Wang J, Qu K, Zhang J, Li L, Bouley DM, Lujan E, Haddad B, Daneshvar K *et al* (2014) m(6)A RNA modification controls cell fate transition in mammalian embryonic stem cells. *Cell Stem Cell* 15: 707–719

18. Lee H, Bao S, Qian Y, Geula S, Leslie J, Zhang C, Hanna JH, Ding L (2019) Stage-specific requirement for Mettl3-dependent m(6)A mRNA methylation during haematopoietic stem cell differentiation. *Nat Cell Biol* 21: 700–709

19. Bertero A, Brown S, Madrigal P, Osnato A, Ortmann D, Yiangou L, Kadiwala J, Hubner NC, de Los Mozos IR, Sadee C *et al* (2018) The SMAD2/3 interactome reveals that TGFbeta controls m(6)A mRNA methylation in pluripotency. *Nature* 555: 256–259

20. Vu LP, Pickering BF, Cheng Y, Zaccara S, Nguyen D, Minuesa G, Chou T, Chow A, Saletore Y, MacKay M *et al* (2017) The N(6)-methyladenosine (m(6)A)-forming enzyme METTL3 controls myeloid differentiation of normal hematopoietic and leukemia cells. *Nat Med* 23: 1369–1376

21. Leppek K, Das R, Barna M (2018) Functional 5′ UTR mRNA structures in eukaryotic translation regulation and how to find them. *Nat Rev Mol Cell Biol* 19: 158–174

22. Faller WJ, Jackson TJ, Knight JR, Ridgway RA, Jamieson T, Karim SA, Jones C, Radulescu S, Huels DJ, Myant KB *et al* (2015) mTORC1-mediated translational elongation limits intestinal tumour initiation and growth. *Nature* 517: 497–500

23. Ireland H, Kemp R, Houghton C, Howard L, Clarke AR, Sansom OJ, Winton DJ (2004) Inducible Cre-mediated control of gene expression in the murine gastrointestinal tract: effect of loss of beta-catenin. *Gastroenterology* 126: 1236–1246

24. van de Wetering M, Sancho E, Verweij C, de Lau W, Oving I, Hurlstone A, van der Horn K, Batlle E, Coudreuse D, Haramis AP *et al* (2002) The beta-catenin/TCF-4 complex imposes a crypt progenitor phenotype on colorectal cancer cells. *Cell* 111: 241–250

25. Willert J, Epping M, Pollack JR, Brown PO, Nusse R (2002) A transcriptional response to Wnt protein in human embryonic carcinoma cells. *BMC Dev Biol* 2: 8

26. Chen J, Huang XF (2009) The signal pathways in azoxymethane-induced colon cancer and preventive implications. *Cancer Biol Ther* 8: 1313–1317

27. Schepers AG, Snippert HJ, Stange DE, van den Born M, van Es JH, van de Wetering M, Clevers H (2012) Lineage tracing reveals Lgr5+ stem cell activity in mouse intestinal adenomas. *Science* 337: 730–735

28. Tirumuru N, Zhao BS, Lu W, Lu Z, He C, Wu L (2016) N(6)-methyladenosine of HIV-1 RNA regulates viral infection and HIV-1 Gag protein expression. *Elife* 5: e15528

29. Hsu PJ, Shi H, He C (2017) Epitranscriptomic influences on development and disease. *Genome Biol* 18: 197

30. Shi H, Zhang X, Weng YL, Lu Z, Liu Y, Li J, Hao P, Zhang Y, Zhang F, Wu Y *et al* (2018) m(6)A facilitates hippocampus-dependent learning and memory through YTHDF1. *Nature* 563: 249–253

31. Han D, Liu J, Chen C, Dong L, Liu Y, Chang R, Huang X, Wang J, Dougherty U, Bissonnette MB *et al* (2019) Anti-tumour immunity controlled through mRNA m(6)A methylation and YTHDF1 in dendritic cells. *Nature* 566: 270–274

32. van Es JH, Haegebarth A, Kujala P, Itzkovitz S, Koo BK, Boj SF, Korving J, van den Born M, van Oudenaarden A, Robine S *et al* (2012) A critical role for the Wnt effector Tcf4 in adult intestinal homeostatic self-renewal. *Mol Cell Biol* 32: 1918–1927

33. Flanagan DJ, Phesse TJ, Barker N, Schwab RH, Amin N, Malaterre J, Stange DE, Nowell CJ, Currie SA, Saw JT *et al* (2015) Frizzled7 functions as a Wnt receptor in intestinal epithelial Lgr5(+) stem cells. *Stem Cell Rep* 4: 759–767

34. Ashton GH, Morton JP, Myant K, Phesse TJ, Ridgway RA, Marsh V, Wilkins JA, Athineos D, Muncan V, Kemp R *et al* (2010) Focal adhesion kinase is required for intestinal regeneration and tumorigenesis downstream of Wnt/c-Myc signaling. *Dev Cell* 19: 259–269

35. Shi H, Wei J, He C (2019) Where, when, and how: context-dependent functions of RNA methylation writers, readers, and erasers. *Mol Cell* 74: 640–650

36. Weng YL, Wang X, An R, Cassin J, Vissers C, Liu Y, Liu Y, Xu T, Wang X, Wong SZH *et al* (2018) Epitranscriptomic m(6)A regulation of axon regeneration in the adult mammalian nervous system. *Neuron* 97: 313–325 e6

37. Nishizawa Y, Konno M, Asai A, Koseki J, Kawamoto K, Miyoshi N, Takahashi H, Nishida N, Haraguchi N, Sakai D *et al* (2018) Oncogene c-Myc promotes epitranscriptome m(6)A reader YTHDF1 expression in colorectal cancer. *Oncotarget* 9: 7476–7486

38. Bai Y, Yang C, Wu R, Huang L, Song S, Li W, Yan P, Lin C, Li D, Zhang Y (2019) YTHDF1 regulates tumorigenicity and cancer stem cell-like activity in human colorectal carcinoma. *Front Oncol* 9: 332

39. Inoki K, Ouyang H, Zhu T, Lindvall C, Wang Y, Zhang X, Yang Q, Bennett C, Harada Y, Stankunas K *et al* (2006) TSC2 integrates Wnt and energy signals via a coordinated phosphorylation by AMPK and GSK3 to regulate cell growth. *Cell* 126: 955–968

40. Cai J, Maitra A, Anders RA, Taketo MM, Pan D (2015) beta-Catenin destruction complex-independent regulation of Hippo-YAP signaling by APC in intestinal tumorigenesis. *Genes Dev* 29: 1493–1506

41. Sato T, Vries RG, Snippert HJ, van de Wetering M, Barker N, Stange DE, van Es JH, Abo A, Kujala P, Peters PJ *et al* (2009) Single Lgr5 stem cells build crypt-villus structures *in vitro* without a mesenchymal niche. *Nature* 459: 262–265

42. Sato T, van Es JH, Snippert HJ, Stange DE, Vries RG, van den Born M, Barker N, Shroyer NF, van de Wetering M, Clevers H (2011) Paneth cells constitute the niche for Lgr5 stem cells in intestinal crypts. *Nature* 469: 415–418